ISSN (Print) 1226-1750
ISSN (Online) 2233-6656
Journal of Magnetics 30(4), 681-687 (2025) https://doi.org/10.4283/JMAG.2025.30.4.681

Study on Winding Method for Improving Accuracy of Variable Reluctance Resolver

Jong-Min Kim, Sung-Hyun Yoon, and Chang-Sung Jin*

Department of Electrical Engineering, Wonkwang University, Iksan-si 54538, Republic of Korea

(Received 15 December 2025, Received in final form 26 December 2025, Accepted 26 December 2025)

Electric vehicle (EV) drive systems primarily utilize Permanent Magnet Synchronous Motors (PMSMs) due to their high-power density and efficiency. Precise rotor position detection is essential for high-performance vector control of PMSMs; therefore, resolvers are well-suited as position sensors in EVs owing to their simple structure, durability, and environmental robustness. However, significant position errors can lead to reduced output torque, increased torque ripple, and mechanical vibration. Consequently, this paper proposes two novel winding methods—Overlapping winding and Parallel winding—to enhance the position accuracy of Variable Reluctance (VR) resolvers. The position error was analyzed using Finite Element Analysis (FEA) via Ansys Maxwell and an RDC tracking method implemented in Excel VBA. The results confirmed that the proposed methods are effective in significantly improving precision.

Keywords : accuracy, position sensor, variable reluctance resolver, winding method

1. Introduction

With the increasing adoption of electric vehicles (EVs) and hybrid electric vehicles (HEVs), the demand for position sensors used in drive motor control is also growing. Compared to encoders, resolvers offer superior durability and environmental resistance including high temperatures, vibrations, shocks, and humidity making them highly reliable in harsh operating conditions. As a result, resolvers are widely used in modern electro-mechanical systems [1–3].

Resolvers are primarily classified into two types: Wound Rotor (WR) and Variable Reluctance (VR). The WR type resolver contains two quadrature output windings on the stator and an excitation winding on the rotor. This configuration requires a rotary transformer and a frame to transfer the excitation voltage to the rotor winding, resulting in a more complex structure. Consequently, the axial length is increased, and the manufacturing process becomes more complicated [4]. In contrast, the VR-type resolver features both the excitation winding and two quadrature output windings on the stator, and has a rotor composed of salient poles. Since it does not require a rotary transformer, the VR resolver offers a more compact axial structure and a simpler mechanical design [5–7].

The VR resolver estimates the rotor position based on the voltage induced in the output windings, and the distribution of these windings plays a critical role in determining accuracy. By using a parallel circuit that allows the winding distribution to be defined with sub-degree precision, the accuracy can be improved. Furthermore, the overlapping winding method mitigates imperfect quadrature between the SIN and COS signals, thereby enhancing accuracy.

2. Principle of VR Resolver and Position Estimation Method

Fig. 1 illustrates the internal wiring diagram of a VR resolver. As the rotor with salient poles rotates, the length of the air gap varies accordingly. This variation leads to changes in the air-gap reluctance, resulting in a position-dependent transformation ratio.

When an AC voltage is applied through the excitation winding R1–R2 on the left side, voltages are induced in the output windings S1–S3 and S2–S4. As shown in Fig. 2, the excitation winding produces an AC waveform, while the output windings generate sinusoidal (SIN) and cosinusoidal (COS) waveforms. These output voltages

*Corresponding author: Tel: +82-63-850-6298
e-mail: csjin76@wku.ac.kr

can be mathematically expressed by Eqs. (1)-(3) [8].

$$E_{R1-R2} = E\ sin\ \omega t \tag{1}$$

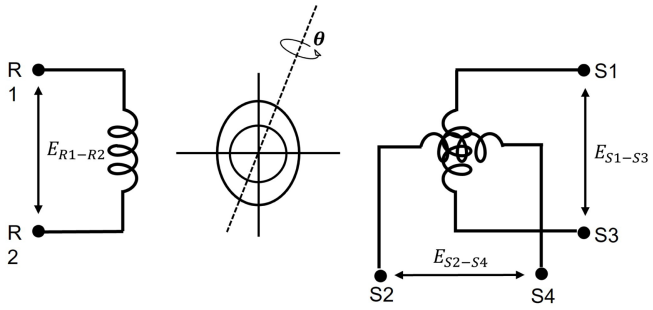

Fig. 1. Main principle of resolver.

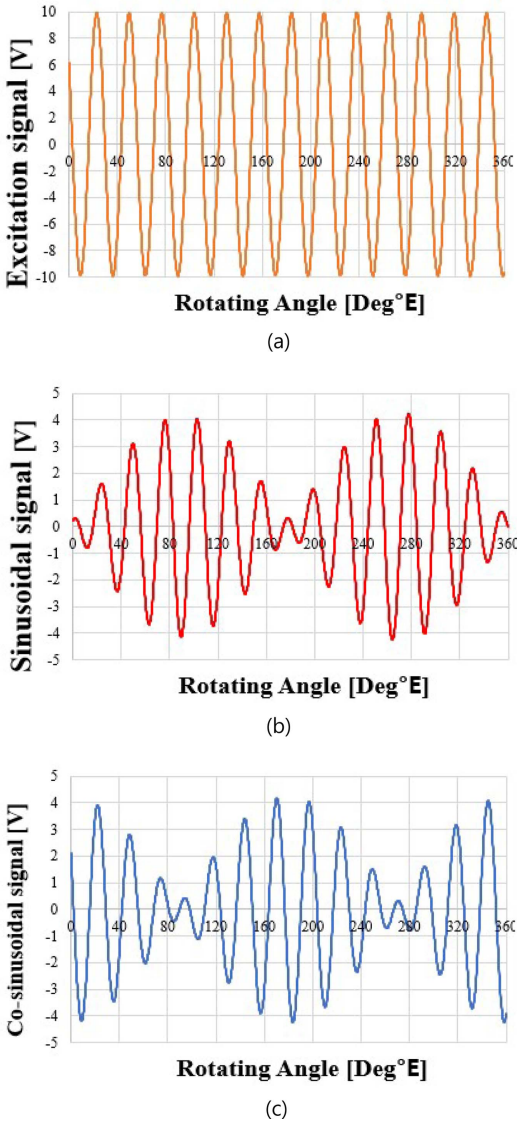

Fig. 2. (Color online) Input and output signal waveforms: (a) Excitation waveform, (b) SIN output, (c) COS output.

$$E_{S1-S3} = KE_{R1-R2}\cos\theta \tag{2}$$

$$E_{S2-S4} = KE_{R1-R2}\sin\theta \tag{3}$$

Where E is the amplitude of the applied excitation voltage, K is the transformation ratio, and θ is the rotor angle.

The VR resolver allows rotor position estimation based on the envelope of the SIN and COS output voltages using an arctangent function, as given in Eq. (4).

$$\theta = \tan^{-1}\frac{E_{S2-S4}}{E_{S1-S3}} \tag{4}$$

In practical applications, a Resolver-to-Digital Converter (RDC) typically employs a tracking method to determine position. This method operates a feedback loop such that the error between the estimated angle and the actual rotor angle converges to zero.

$$\begin{aligned} &KE\sin\omega t\,(\sin\theta\cos\phi - \cos\theta\sin\phi) \\ &\quad = KE\sin\omega t\sin(\theta-\phi) \end{aligned} \tag{5}$$

As shown in Fig. 3, the output signals from the resolver are input to the RDC, where they are multiplied by the sine and cosine of the current estimated angle ϕ, respectively. The difference between the two results yields Eq. (5). After demodulation, only the fundamental component remains, which is expressed as $KE\sin(\theta-\phi)$. Assuming that the estimated angle is close to the actual angle, the signal can be approximated as Eq. (6) [9].

$$KE\sin(\theta-\phi) \approx KE(\theta-\phi) \tag{6}$$

In this study, the tracking algorithm was implemented using a VBA script in Microsoft Excel, and the position error was calculated using the output voltage data

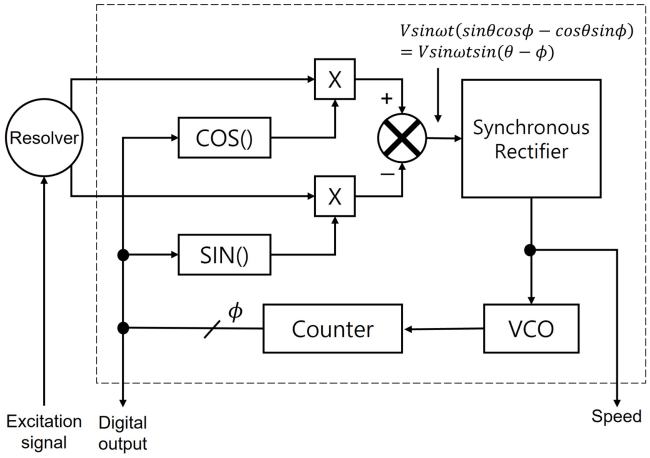

Fig. 3. Block diagram of RDC.

obtained from FEA in Ansys Maxwell.

3. Specifications and Parameters of the Analysis Model

The simulation model is a 5-pole, 12-slot VR resolver, as shown in Fig. 4. The parameters of the simulation model are listed in Table 1, and the proposed winding methods were applied based on this model.

Table 1. Design parameters of the VR resolver analysis model.

Parameter	Value	Unit
Poles / Slots	5 / 12	-
Rotor / Stator Outer Diameter	30 / 50	mm
Stator Yoke	11.9	mm
Teeth Width	8	mm
Slot Opening	2	mm
Air Gap	0.5	mm
Stack Length	7	mm
Input Voltage	7	V_{rms}
Input Frequency	10	kHz
Output Voltage	1.8 – 2.2	V_{rms}

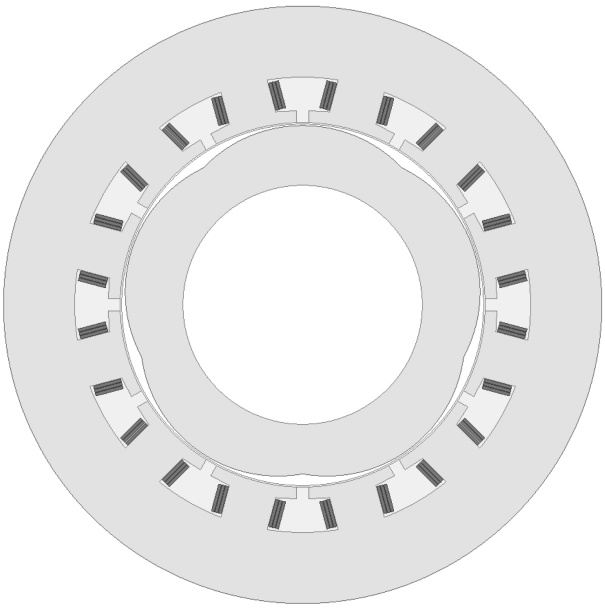

Fig. 4. Analysis model of a 5-pole, 12-slot VR resolver.

4. Winding Method for Improving Accuracy of the VR Resolver

The VR resolver has both excitation and output windings placed on the stator. The number of turns for the excitation winding can be determined using Eq. (7). Eq. (8) represents the condition required to obtain a normal output voltage. If $Z = 4p$ is satisfied when $P_w = p$, or if $(Z \pm 2P_w)/2 = p$ is satisfied, the output voltage will exhibit p sinusoidal cycles per mechanical rotation. The combination of rotor poles and slots that satisfies this is shown in Table 2.

Table 2. Pole-slot combinations and winding pole pair numbers of the VR resolver.

Stator Teeth	Rotor Poles			
	$p_w = 1$	$p_w = 2$	$p_w = 3$	$p_w = 4$
10	4, 6	3, 7	2, 8	1, 9
12	5, 7	4, 8	3, 9	2, 10
14	6, 8	5, 9	4, 10	3, 11
16	7, 9	6, 10	5, 11	4, 12
18	8, 10	7, 11	6, 12	5, 13
20	9, 11	8, 12	7, 13	6, 14
22	10, 12	9, 13	8, 14	7, 15
24	11, 13	10, 14	9, 15	8, 16

$$N_k = N_e \cos[(k-1)\,\pi] \tag{7}$$

Where N_k is the number of turns in the k-th slot, N_e is the total number of excitation turns, and k is the slot number.

$$P_w = p \quad or \quad \frac{Z \pm 2P_w}{2} = p \tag{8}$$

Where P_w is the winding pole pair number, p is the number of rotor poles, and Z is the number of stator slots.

The output winding distribution is determined by the pole-slot configuration and the maximum number of

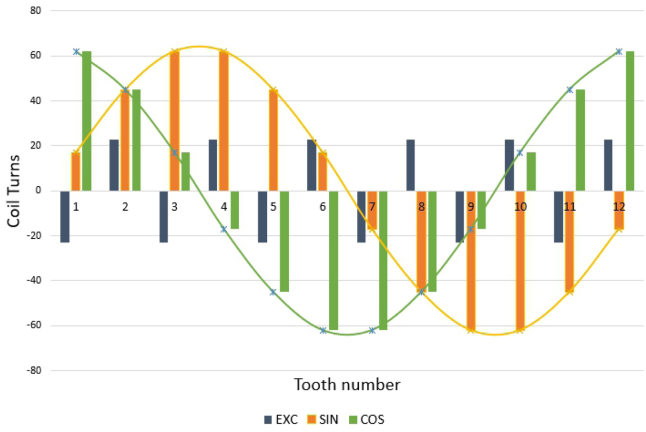

Fig. 5. (Color online) Winding distribution of the analysis model (α = 15°).

turns. As shown in Fig. 5, the two output windings are configured with a 90° phase difference, forming SIN and COS patterns. To generate such a distribution, the winding function incorporating P_w is formulated as Eq. (9) [10].

$$N_i|_{SIN} = N_{max} \sin\left[(k-1)\frac{P_w\pi}{(Z/2)} + \alpha\right]$$
$$N_i|_{COS} = N_{max} \cos\left[(k-1)\frac{P_w\pi}{(Z/2)} + \alpha\right] \quad (9)$$

Eq. (9) is a modified form of the conventional winding function, in which a phase shift angle α is introduced and N_{max} represents the maximum number of turns. This allows the magnetic field distribution to be shifted by α degrees. By applying Eq. (9) to the winding design and performing finite element analysis (FEA), the resulting winding distribution and output voltage of the analysis model were obtained, as shown in Table 3 and Fig. 5 and Fig. 6. Since fractional turns cannot be physically implemented, the calculated values were rounded to the nearest integer prior to simulation, as reflected in Table 3. The input voltage for the simulation was set to 7 V_{rms}, and the maximum number of output winding turns was determined to be 64 turns to meet the output specification of 2 V_{rms} ±10%. If the coil resistance or impedance is lower than the target value, the number of output turns can be increased accordingly; in such cases, the transformation ratio must be adjusted downward. Conversely, if the impedance is higher than desired, the number of output turns can be reduced, and the transformation ratio increased to meet the specification [11].

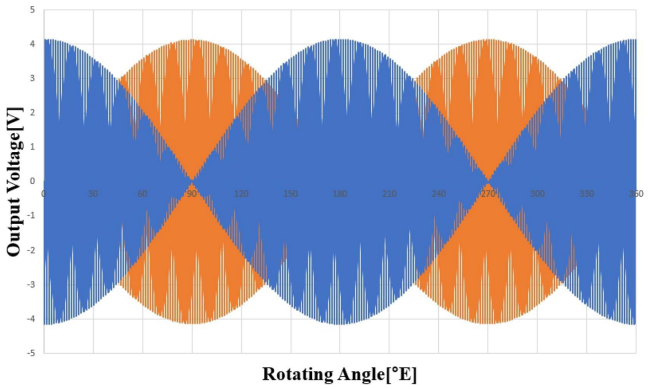

Fig. 6. (Color online) Output voltage of the analysis model.

Table 3. Calculated and rounded turns of Conventional winding method.

Teeth Number	Sin coil		Cos coil	
	Calculated	Rounded	Calculated	Rounded
1	16.6	17	61.8	62
2	45.3	45	45.3	45
3	61.8	62	16.6	17
4	61.8	62	16.6	17
5	45.3	45	45.3	45
6	16.6	17	61.8	62
7	16.6	17	61.8	62
8	45.3	45	45.3	45
9	61.8	62	16.6	17
10	61.8	62	16.6	17
11	45.3	45	45.3	45
12	16.6	17	61.8	62

4.1. Parallel Winding Method

When Eq. (9) is evaluated, it yields fractional numbers of turns, as shown in Table 3. To improve the accuracy of the VR resolver, this paper proposes a method of connecting output windings in parallel. In a parallel winding structure, the number of turns increases in proportion to the number of parallel paths, allowing the implementation of non-integer (fractional) turns [12]. Eq. (9) can be reformulated by multiplying it by the number of parallel circuits a, resulting in Eq. (10). The resulting winding distribution for a = 2 is presented in Table 4. By applying parallel winding, fractional turn values such as 0.5 turns can be realized—for example, when a = 2, as shown in Table 4. This allows the actual wound coil to closely approximate the calculated values from Eq. (9), resulting in a more sinusoidally distributed magnetomotive force (MMF), which improves the position accuracy of the VR resolver. However, when a = 2 with the same wire diameter, the resistance decreases by half. Thus, as the number of parallel circuits increases, the total coil resistance decreases inversely with the number of paths. To maintain the desired resistance in a parallel configuration, the wire diameter must be reduced to increase resistance, which can be calculated using Eq. (11).

$$N_i|_{SIN} = aN_{max} \sin\left[(k-1)\frac{P_w\pi}{(Z/2)} + \alpha\right]$$
$$N_i|_{COS} = aN_{max} \cos\left[(k-1)\frac{P_w\pi}{(Z/2)} + \alpha\right] \quad (10)$$

$$D_a = \frac{D_e}{\sqrt{a}} \quad (11)$$

Where a is the number of parallel paths, D_a is the diameter of each conductor when using a parallel path, and D_e is the diameter of the original single conductor.

Table 4. Parallel winding distribution and a = 1 conversion table.

Teeth Number	Sin coil		Cos coil	
	$a=2$	Converted to $a=1$	$a=1$	Converted to $a=1$
1	33	16.5	124	62
2	91	45.5	91	45.5
3	124	62	33	16.5
4	124	62	33	16.5
5	91	45.5	91	45.5
6	33	16.5	124	62
7	33	16.5	124	62
8	91	45.5	91	45.5
9	124	62	33	16.5
10	124	62	33	16.5
11	91	45.5	91	45.5
12	33	16.5	124	62

Table 5. Overlapping winding distribution.

Teeth Number	Sin coil				Cos coil			
1	17	17			62	17	28	17
2	45		28	17	45			
3	62				17			
4	62				17	17	28	17
5	45				45			
6	17				62			
7	17	17			62			
8	45		28	17	45			
9	62				17			
10	62				17	…	…	…
11	45				45			
12	17				62			

4.2. Overlapping Winding Method

Another approach proposed to improve the accuracy of the VR resolver is the overlapping winding method. In this method, turns are distributed by grouping multiple adjacent slots, forming overlapping layers of coils. As a result, SIN and COS waveforms are induced on the output windings. Using the modified winding function, a phase shift of 15° is applied to the magnetic field distribution. The resulting overlapping winding distribution is shown in Table 5, and the actual winding method is illustrated in Fig. 7.

Specifically, the winding is implemented as follows:
- 17 turns are wound across slots 1 through 6
- 28 turns are wound across slots 2 through 5
- The remaining 17 turns are wound across slots 3 and 4

Quadrature error refers to the deviation of the phase difference between the SIN and COS signals from 90°E, and is a type of position error caused by non-ideal characteristics of the resolver [13]. In the conventional winding method, the Sin 180°E point occurred at 8,989 steps (179.78°E) and the Cos 180°E point at 9,018 steps (180.36°E), resulting in a quadrature error of 0.58°E between the two phases. On the other hand, in the case of the proposed overlapping winding method, the Sin 180°E point occurred at 9,010 steps (180.2°E) and the Cos 180°E point at 9,018 steps (180.36°E), resulting in a quadrature error of 0.16°E between the two phases.

4.3. Excel VBA Tracking Program

A position error estimation program was developed by implementing the tracking method shown in Fig. 3 using Excel VBA. Using this program, the maximum and minimum position errors for each winding were estimated to compare and analyze their accuracy. This program estimates the resolver position by using output voltage data obtained from Ansys Maxwell analysis as input. For the angle estimation, a digital estimated angle, ϕ, is input. Eq. (5) is executed by multiplying $\sin(\phi)$ and $\cos(\phi)$ with the two output voltages of the resolver and subtracting the resulting values. The estimated angle is incremented from

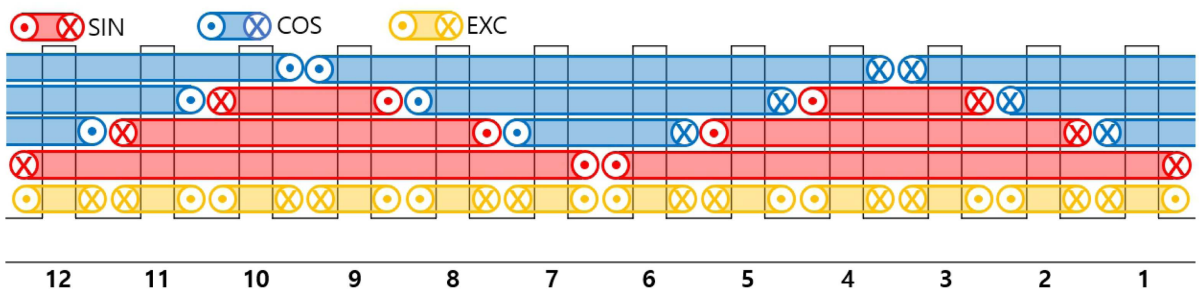

Fig. 7. (Color online) Illustration of the Overlapping winding method.

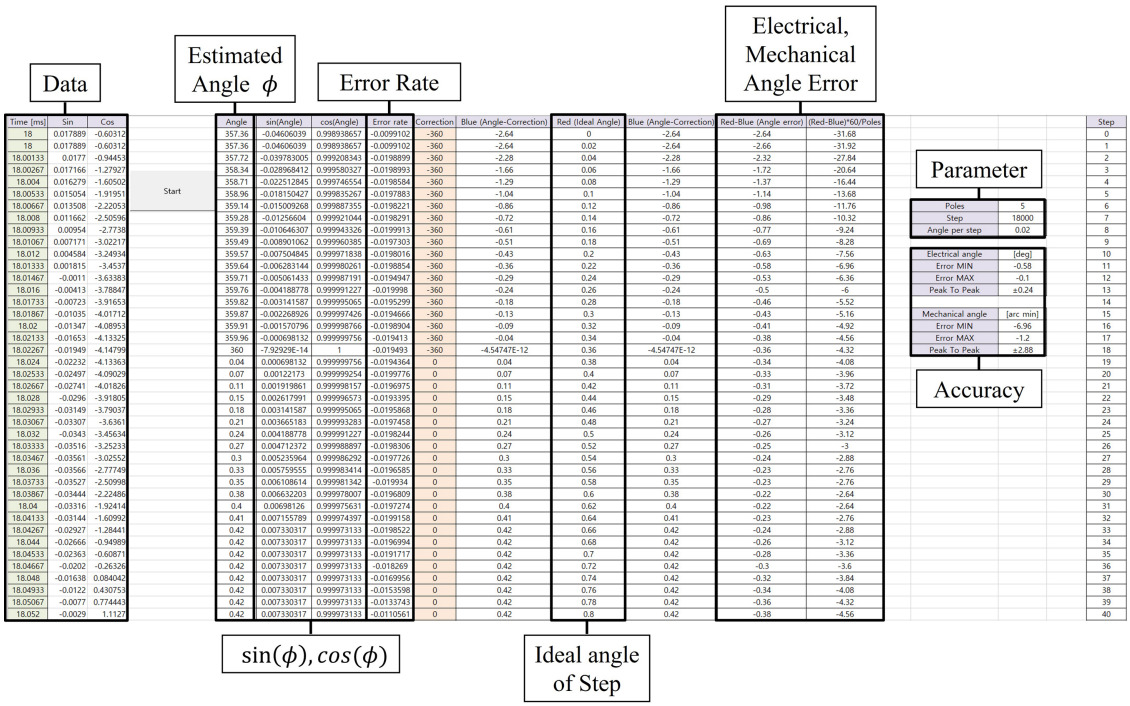

Fig. 8. (Color online) Excel VBA Tracking program.

0° to 360° in specified angular steps until the angle error falls within the allowable tolerance range. Consequently, the estimated angle closely matches the actual angle according to Eq. (6). Finally, the electrical position error is calculated by comparing the estimated angle with the ideal angle.

5. Simulation Results

Accuracy is defined as the range of position error, calculated as the difference between the maximum and minimum values. Mechanical angle accuracy is expressed in arcmin (′), a finer unit than degrees (°). The simulation result of the conventional winding model shows an electrical angle accuracy of ±0.24°, corresponding to ±2.88 arcmin in mechanical angle. Fig. 9 presents the position error for the parallel winding configuration, where (a) shows the conventional winding and (b) shows the parallel winding with a = 2.

In the case of the parallel winding method, when the number of parallel paths was set to 2, an accuracy improvement of approximately 4.2% was observed compared to the conventional winding. This improvement is attributed to the parallel winding's ability to emulate fractional turn effects, allowing the implemented winding distribution to more closely approximate the ideal values calculated from Eq. (9).

For the overlapping winding method, an improvement of approximately 10.4% in accuracy was observed due to the reduction in quadrature error. Simulation results indicate that the quadrature error between the SIN and COS phases was 0.58°E in the conventional winding and 0.16°E in the overlapping winding. This reduction in quadrature error contributes to the overall improvement in

Table 6. Comparison of accuracy according to winding methods.

Items		Conventional	Overlapping	Parallel	Unit
Electrical Angle	Position error Min	-0.28	-0.26	-0.27	°
	Position error Max	0.2	0.17	0.19	°
	Accuracy	±0.24	±0.215	±0.23	°
Mechanical Angle	Position error Min	-3.36	-3.12	-3.24	′
	Position error Max	2.4	2.04	2.28	′
	Accuracy	±2.88	±2.58	±2.76	′

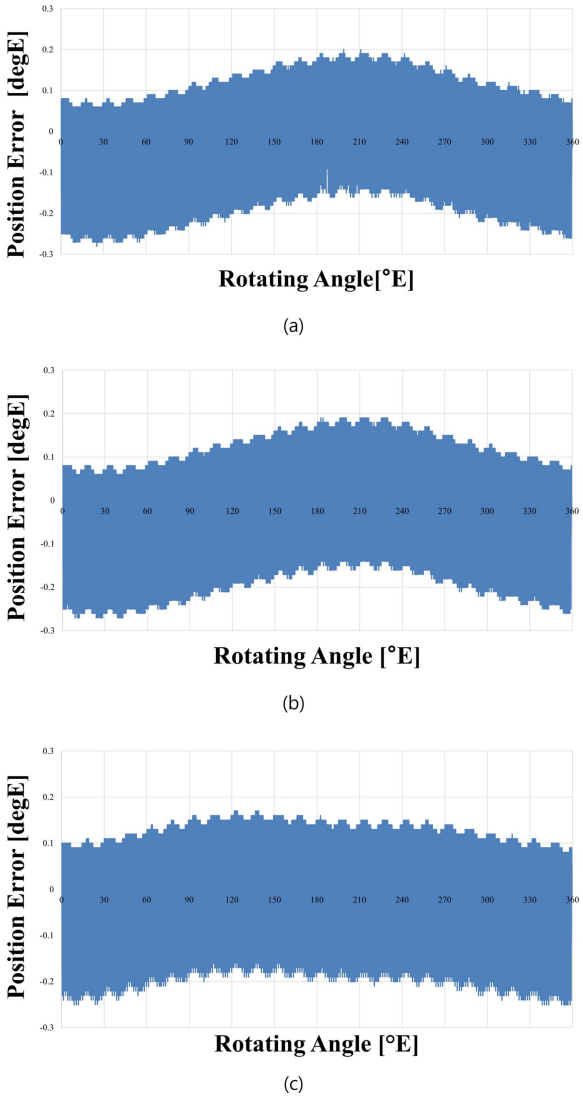

Fig. 9. (Color online) Electrical angle position error for the proposed windings: (a) Conventional winding, (b) Parallel winding with a = 2, (c) Overlapping winding.

position accuracy. The comparison of accuracy according to winding method is shown in Table 6.

6. Conclusions

In this study, winding methods for improving the accuracy of variable reluctance resolvers were investigated. To enhance position accuracy, two approaches were proposed based on the conventional winding function: the parallel winding method and the overlapping winding method. The effect of these methods on accuracy was evaluated by extracting position error using a tracking algorithm implemented in Excel VBA, based on finite element method simulation results obtained from Ansys Maxwell. The results confirmed that the proposed winding techniques effectively contribute to improving the accuracy of the VR resolver.

Acknowledgements

This paper was supported by Wonkwang University in 2024.

References

[1] V. Abramenko, J. Stenbäck, I. Petrov, and J. Pyrhönen, 2024 International Conference on Electrical Machines (ICEM), Torino, Italy (2024) pp. 1-7.
[2] X. Ge, Z. Q. Zhu, R. Ren, and J. T. Chen, IEEE Trans. Ind. Appl. **52**, 2872 (2016).
[3] J. Kang and G. Choi, 2024 IEEE 21st Biennial Conference on Electromagnetic Field Computation (CEFC), Jeju, Korea (2024) pp. 1-2.
[4] S. Hajmohammadi, R. Alipour-Sarabi, Z. Nasiri-Gheidari, and F. Tootoonchian, 2019 10th International Power Electronics, Drive Systems and Technologies Conference (PEDSTC), Shiraz, Iran (2019) pp. 166-171.
[5] F. Tootoonchian, IEEE Sens. J. **18**, 5284 (2018).
[6] F. Tootoonchian, IEEE Sens. J. **16**, 7464 (2016).
[7] Z. Nasiri-Gheidari, IEEE Trans. Energy Convers. **32**, 276 (2016).
[8] C.-S. Jin, I.-S. Jang, J.-N. Bae, J. Lee, and W.-H. Kim, IEEE Trans. Magn. **51**, 1 (2015).
[9] H.-B. Lim, Ph.D. Dissertation, Adaptive Compensation of Resolver Position Error for High-Performance HEV Motor Control, Hanyang University, Seoul, Republic of Korea (2010).
[10] X. Ge, Z. Q. Zhu, R. Ren, and J. T. Chen, IEEE Trans. Magn. **51**, 1 (2014).
[11] I.-J. Yang, J. Lee, and C.-S. Jin, J. Korean Magnetics Society **34**, 266 (2024).
[12] L. H. Dixon, Magnetics Design Handbook (2000) R6-1 - R6-8.
[13] D. C. Hanselman, IEEE Trans. Ind. Electron. **37**, 556 (2002).